Design of an enhanced adaptive hybrid controller for switched reluctance motors

M.W. Arab[*], X. Rain[*], M. Hilairet[°], P. García Estébanez[#], H. Hannoun[#], C. Marchand[*]
[*]LGEP/SPEE Labs; CNRS UMR8507; SUPELEC; Univ Pierre et Marie Curie-P6; Univ Paris Sud-P11, 91192 Gif sur Yvette, France
[°]FEMTO-ST, CNRS UMR 6174, University of Franche-Comte, F-90010 Belfort, France
[#]Technocentre Renault, 1 avenue du Golf - 78288 Guyancourt cedex, France
mohammad-waseem.arab@lgep.supelec.fr, xavier.rain@lgep.supelec.fr, mickael.hilairet@univ-fcomte.fr, pablo.garcia@renault.com, hala.hannoun@renault.com, claude.marchand@lgep.supelec.fr

***Abstract*— This paper deals with current control in switched reluctance motors with an objective of maximizing torque generation. First, the structure of a hybrid controller is recalled. This controller, which is a combination of an on-off and a PI controller, is efficient for controlling SRMs using square wave current pulses. Next, advantages and drawbacks of this controller with high current dynamics are detailed. Finally, an enhanced structure of this controller overcoming these drawbacks is presented. The advantages of the new controller are detailed and validated by simulation.**

Keywords—switched reluctance motors; current control; hybrid controller; PI controller; Hysteresis controller

I. INTRODUCTION

Switched Reluctance Motors (SRMs) have been known since the 19th century. This type of motors possesses numerous advantages such as low fabrication cost, mechanical robustness and fault-tolerance capabilities. Yet, their application was limited until the recent advancements in electronics and digital control. Nowadays, SRMs are gaining increased attention in both scientific and industrial fields.

Considering their aforementioned advantages, many automobile manufacturers are considering SRMs for electric propulsion purposes [1]. Nevertheless, they are confronted by three major challenges, namely torque ripple, acoustic noise and strong dependence on the rotor position [2, 3, 4]. Also, the electromagnetic characteristics of this machine are nonlinear which renders the current control relatively complicated comparing to other types of motor [5].

Several types of controllers have been reported in the literature. These methods can be classified to linear methods, e.g. PI [6], or nonlinear methods, e.g. hysteresis [7], sliding mode [8], passivity [9] or back-stepping [10]. In any case, the current controller must take the nonlinear nature of the SRM into account. Naturally, hysteresis controller is one of the first choices to be considered given its simplicity, robustness and dynamic response. However, its switching nature yields a control signal with a rich frequency spectrum that can excite multiple vibration modes of the motor [11]. Also, software implementation of this controller by means of Digital Signal Processors (DSP) can lead to current fluctuations increasing torque ripple. The regular Proportional-Integral (PI) controller presents less acoustic noise and a smoother control signal but is not sufficiently dynamic at mid-range speeds. In [12], the authors propose a solution named "hybrid controller" (HC) which combines an on-off and a PI controller. This structure allows for a fast dynamic response as well as a more stable regulation at steady state. Nevertheless, this controller has certain issues when used with SRMs that have high current dynamics. The aim of this paper is to address these issues by proposing a new structure of the HC as well as validating its effectiveness by simulation.

This article is organized in the following order: in section II, the structure of the hybrid controller is recalled and its advantages are presented. Section III presents drawbacks of the hybrid controller when used with SRMs that have high current dynamics. Section IV presents a newer version of this controller adapted to this type of motors. Finally, section V shows simulation results of the developed structure.

II. THE HYBRID CONTROLLER

As mentioned above, this current controller resulted from the combination of both on-off and PI controllers (for more details, see [12]). Fig. 1 shows the operation principle. A threshold current band $\pm\Delta i$ is defined around the current reference which will determine the operation mode of the HC among two possible cases:

- Mode 1: The HC debuts in the on-off mode (or single pulse mode) which stays in effect as long as the current is outside the predefined threshold band. This mode is reengaged whenever the current error exceeds Δi.
- Mode 2: When the current is inside the threshold band, the PI controller takes over the control. Output voltage continuity is assured when switching to the PI controller through the selection of the integral term initial value (S_{ini}) as follows:

$$S_{ini} = V_{dc} - K_p (i^* - i) \quad (1)$$

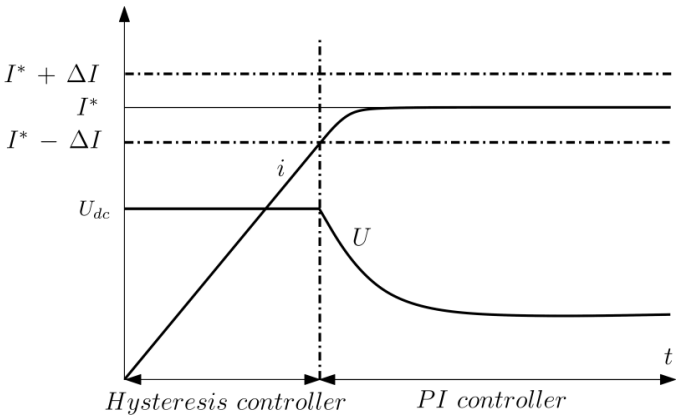

Fig. 1 Hybrid controller operation principle

When the current reference is reassigned to zero, a demagnetization phase is started by applying full negative voltage -V_{dc} until the phase current is equal to zero (seen as mode = –1). Fig. 2 presents a simulation of the hybrid controller at a speed equal to 75% of Ω_l which is the speed limit after which the current control capability is lost due to the increment of the back electromotive force (back-emf). The PI component is configured for a closed loop response of a second order system with ω_n =3200 rad/s and ξ = 0.85 to respect the desired stability margins.

The hybrid controller presents a clear advantage at average speeds compared to the regular PI controller when the back-emf is relatively high. In such case, the hybrid controller achieves a faster current response without scarifying its stability margins.

III. Drawbacks of the Hybrid Controller

In spite of the previously mentioned advantages, some issues were experienced when using the HC with high power SRMs as the case of the studied prototype. Compared to the one studied in [12], current evolution rate is much higher. This fact brings to attention some weak points in the structure of the HC which are detailed in this section.

A. Current fluctuation

At some operating points, the hybrid controller fails to quickly stabilize the current within the threshold band. This leads to voltage and current fluctuations which in turn increases torque ripple and acoustic noise. Fig. 3 shows one case where multiple mode changes take place before finally stabilizing at mode 2. Increment of the current band is not an acceptable solution given that a configuration suitable for mid-range and low currents will degrade the performance at higher currents. Also, starting with full DC voltage at low currents causes an overshoot that is difficult to overcome when switching to the PI controller. This problem is shown in Fig. 4 in which a simulation of the HC is done at a current reference 15% of i_{max}.

B. Integratral term intialisation

Equation (1) calculates the integrator initial value of the PI in mode 2. Yet it was found that (1) overcharges the integrator causing a current overshoot. This problem can be seen clearly in Fig 3.

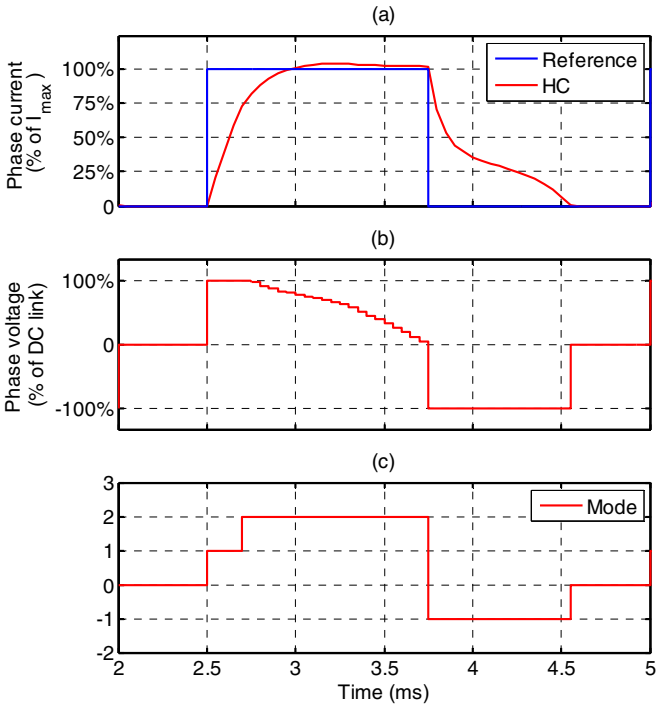

Fig. 2. Simulation of the HC at 75% of Ω_l , mode 1: hysteresis, mode 2: PI. ($\Delta i = 0.2i^*$).

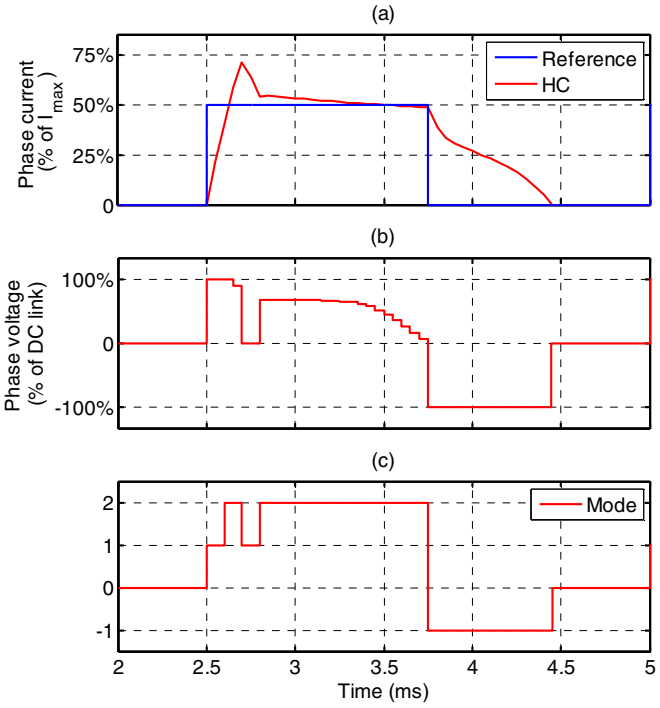

Fig. 3. Simulation of the HC at 75% of Ω_l , mode 1: hysteresis, mode 2: PI. ($\Delta i = 0.2i^*$)

C. *Sensibility to output delay*

The implementation of the controller on a DSP will present a delay of one sample time on the control signal. According to [13], controller output calculated based on variables measured at t_k will be applied at t_{k+1} leading to the desired value of the controlled variable at t_{k+2}. Therefore, it seems logic to calculate the output based on predicted variables at t_{k+1} instead of t_k. Also, this delay cannot be neglected at higher speeds where a limited number of samples are available during an electric cycle. Fig. 5 presents the effect of this delay on the case simulated in Fig. 3.

In the next section, a newer structure is presented in which the previous drawbacks are treated.

IV. Enhanced Hybrid Controller (EHC)

The EHC is composed of three components: the current predictor, the state machine and the PI controller. Fig. 6 presents the block diagram of the EHC. In the coming section, these components are detailed as well as the controller's overall operation principle.

A. *Current predictor*

The electric model of one phase of the machine is given as:

$$u = R_{ph}\, i + L(i,\theta_e)\, di/dt + E(i,\theta_e) \qquad (2)$$

where R_{ph} is the phase resistance, i is the phase current, L is the phase incremental inductance and E is the back-emf. Discretizing (2) using forward Euler method gives (3). Rewriting (3) yields an approximated prediction of the current at the next sample times i_{k+1}. and i_{k+2} as follows:

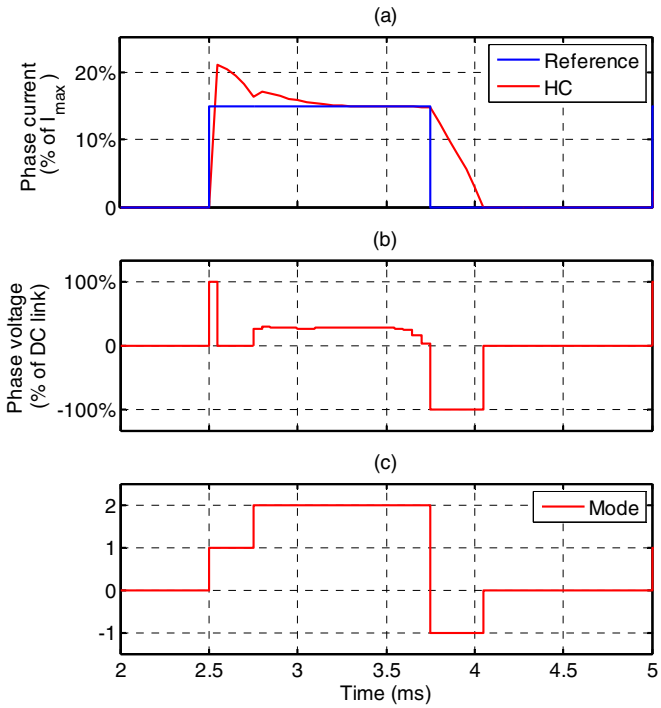

Fig. 4. Simulation of the HC at 75% of Ω_l , mode 1: hysteresis, mode 2: PI. ($\Delta i = 0.2i^*$)

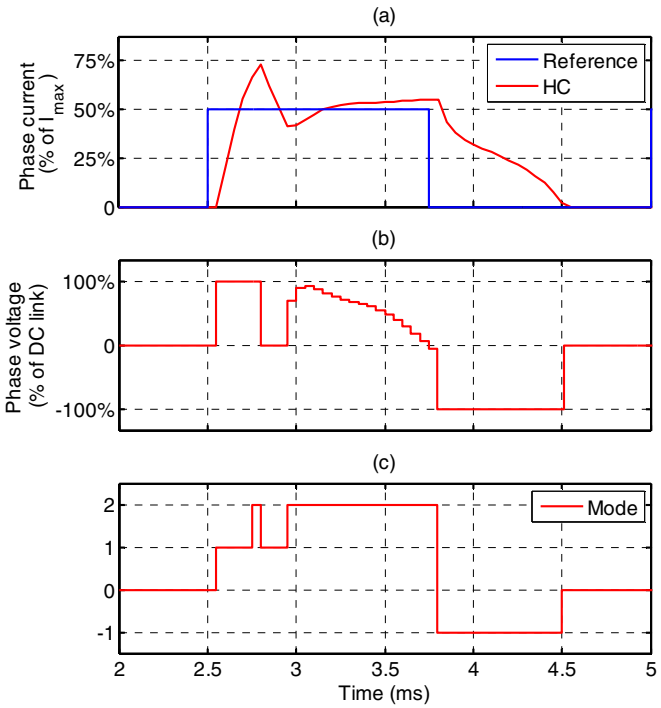

Fig. 5. Simulation of the HC at 75% of Ω_l with an output delay of one sample time, mode 1: hysteresis, mode 2: PI. ($\Delta i = 0.2i^*$)

$$u_k = R_{ph}\, i_k + (i_{k+1} - i_k)\, L_k/T_e + E_k \qquad (3)$$

$$i_{k+1} = i_k + (u_k - R_{ph}\, i_k - E_k)\, T_e/L_k \qquad (4)$$

$$i_{k+2} = i_{k+1} + (u_{k+1} - R_{ph}\, i_{k+1} - E_{k+1})\, T_e/L_k \qquad (5)$$

Replacing u_{k+1} with V_{dc} in (5) gives a prediction of i_{k+2} in the case of applying full DC voltage at the next time sample which is important to determine whether or not to continue in full DC voltage mode. Therefore, it is also necessary to predict both the inductance and the back-emf represented by the terms L_{k+1} and E_{k+1}. These two variables are obtained by linear interpolation of two look-up tables using i_{k+1} and the predicted electric position $\theta_{e,k+1}$ computed from (6).

$$\theta_{e,k+1} = \theta_{e,k} + \omega_e\, T_e \qquad (6)$$

B. *State machine*

The EHC employs a state machine to determine the output voltage in terms of the measured and predicted variables. Four states are defined, namely: magnetization, intermediate step, PI and demagnetization. The state diagram is presented in Fig. 7.

C. *PI controller*

The PI controller employed has the same principle as in [3]. The controller's gains are adapted to the machine inductance on-line as follows:

$$K_i = L(\theta_e,i)\, \omega_n^2,\ K_p = 2\xi\, L(\theta_e,i)\, \omega_n - R_{ph} \qquad (7)$$

The adaptation of the gains allows for conserving a fixed closed-loop dynamics (ω_n =3200 rad/s, ξ = 0.85). One important point to be considered is the initialization of the integral term. As the PI controller is activated when the current

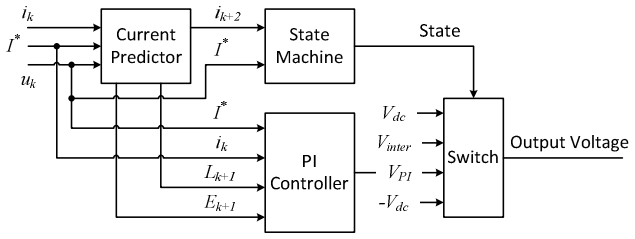

Fig. 6. Block diagram of the EHC

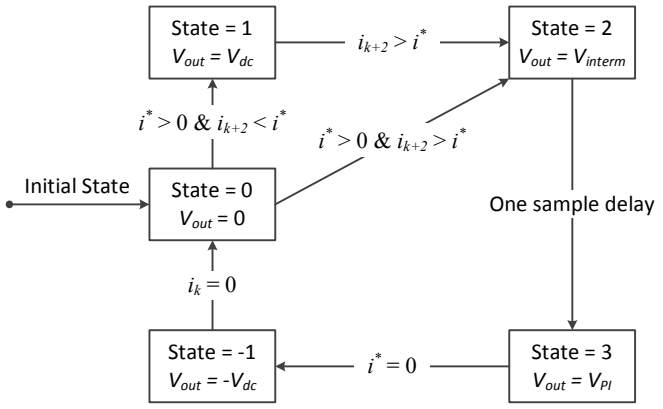

Fig. 7. Diagram of the state machine

reaches to its reference, the initial state is calculated to assure the stability of the current at this value. Compared to the previous work where the integrator is initialized in order to assure the voltage continuity (see (1)), here this is achieved by imposing the condition $di/dt = 0$ as presented in (8).

$$u = R_{ph}\, i + L(i,\theta_e)\, di/dt + E(i,\theta_e) = K_p\,(i^* - i) + S_{ini}$$
$$di/dt = 0 \rightarrow S_{ini} = -K_p\,(i^* - i) + R_{ph}\, i + E \qquad (8)$$

D. EHC principle of operation

In Fig 8, the operating principle of the EHC is presented over one electric cycle. The current regulation proceeds through three states as follows:

- State = 1: The output voltage equals V_{dc}. This state, however, is bypassed in case $i_{k+2} > i^*$ when applying full DC voltage at the next step ($u_{k+1} = V_{dc}$) to avoid current overshoot.
- State = 2: This state is applied for only one sample period. The output voltage is computed from (3) so that the current i_{k+1} is equal to the reference current i^*. This ensures that the current is near the reference value when activating the PI controller.
- State = 3: In this state, the PI controller assumes the current control until the current reference is set to zero.
- State = –1: Here the output voltage is forced to $-V_{dc}$ until the phase current is completely extinguished.

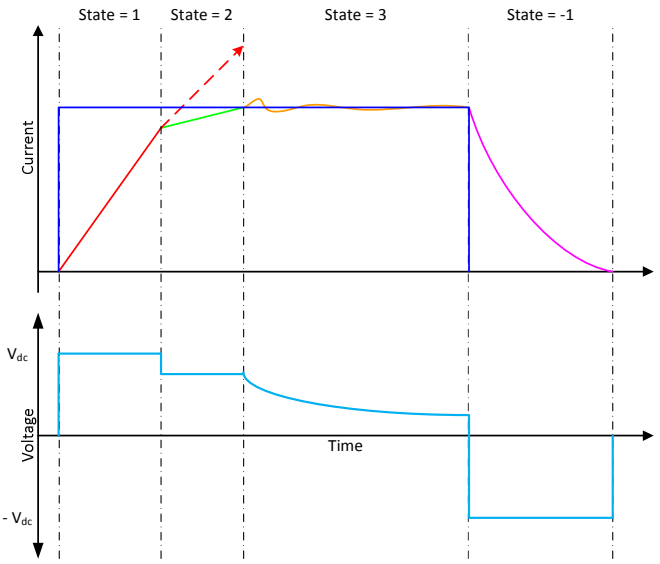

Fig. 8. EHC operation during one electric cycle

V. Simulation Results

The EHC effectiveness has been extensively studied by simulation using MATLAB/Simulink software suite. The control system was simulated at a sampling frequency of 20 kHz. The inductance and electromotive force functions were implemented in form of look-up tables and were pre-calculated using finite elements method [5, 14].

In Fig 9, a simulation of both the HC and the EHC is

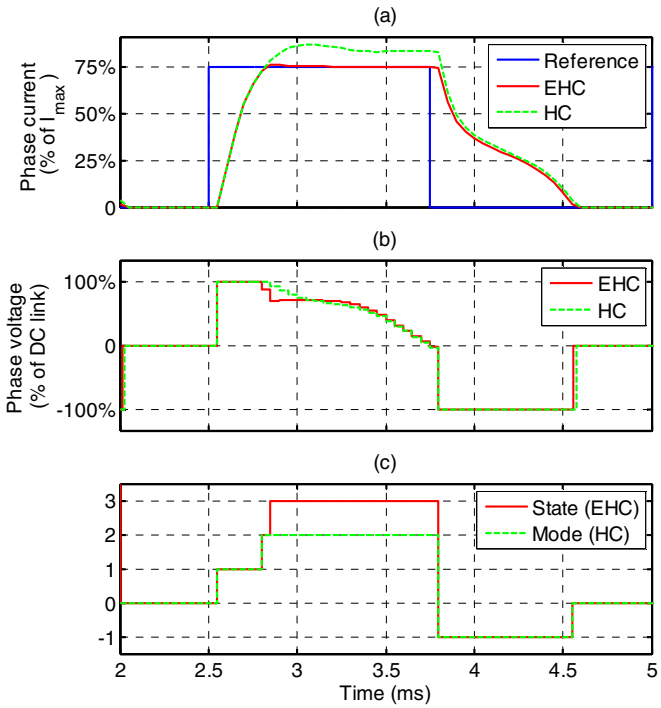

Fig. 9. Simulation of both the HC and the EHC at 75% of Ω_l. i^* = 75% of the phase maximum current.

conducted at 75% of Ω_l. Here, the advantage of the EHC is clear as the current and voltage fluctuations are not present. Also, the initialization of the integrator of the PI controller using (8) allows for a smoother transition without causing any overshoot. Fig. 10 presents a simulation of the EHC at 100% of Ω_l and maximum phase current. The same conclusions as in the case of Fig. 9 can be made which demonstrates furthermore the effectiveness of the EHC at the limits of current control.

Simulation of the EHC at a lower current reference was conducted. Fig 11 displays a simulation at 75% of Ω_l with a

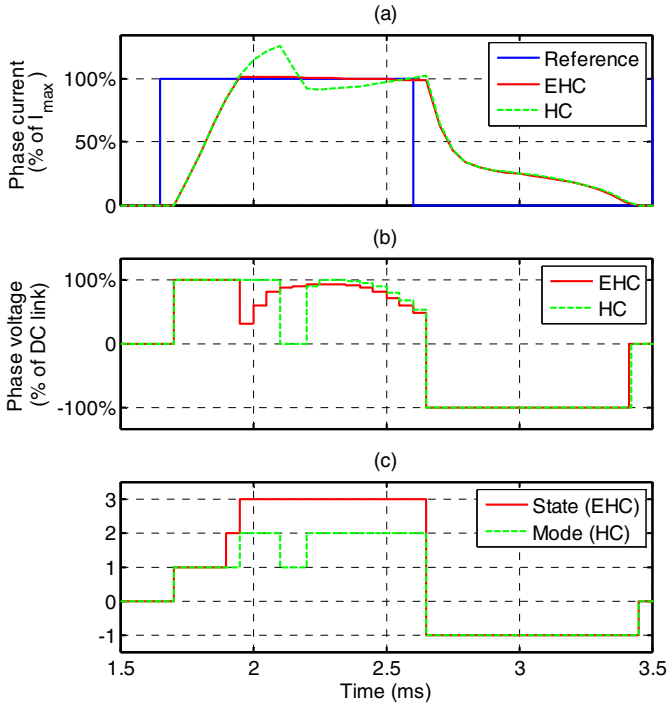

Fig. 10. Simulation of both the HC and the EHC at 100% of Ω_l. i^* = 100% of the phase maximum current.

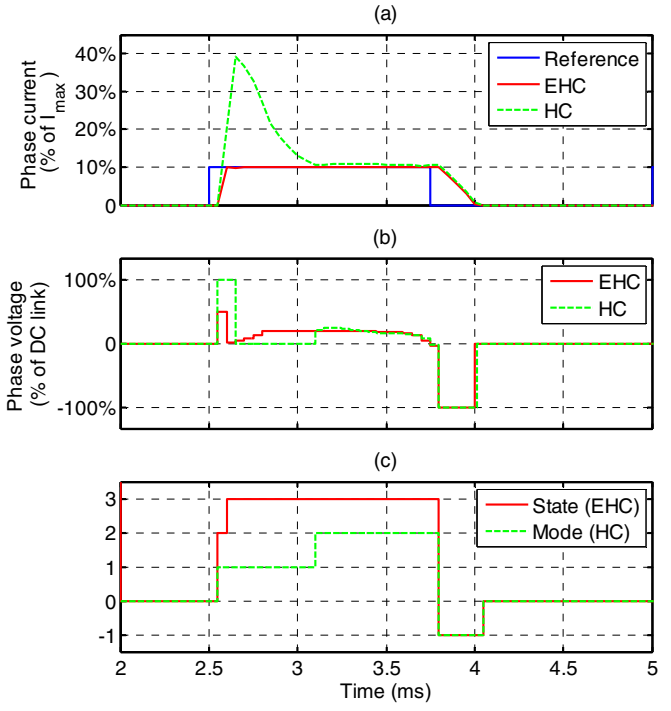

Fig. 11. Simulation of both the HC and the EHC at 75% of Ω_l. i^* = 10% of the phase maximum current.

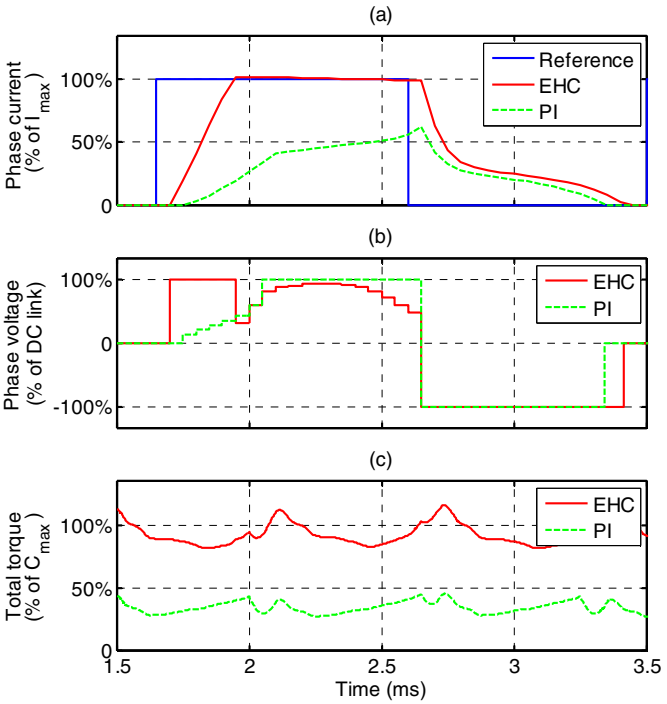

Fig. 12. Comparing the EHC to the PI at at 100% of Ω_l. i^* = 100% of the phase maximum current.

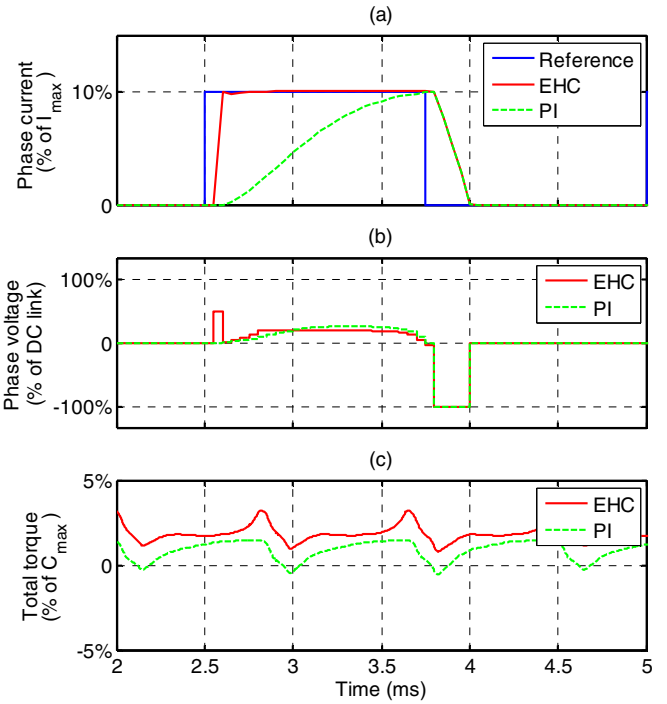

Fig. 13. Comparing the EHC to the PI at at 75% of Ω_l. i^* = 10% of the phase maximum current.

low current reference. It is noted that state 1 (full DC voltage) was avoided as it would cause current overshoot. Also, the intermediate voltage step enables the phase current to be at its reference when switching to the PI thus limiting its role to disturbance rejection.

To further show the advantage of the EHC, its performance was compared to that of the PI on two operation points. In Fig. 12, the two controllers were compared at 100% of Ω_l and with maximum current reference. In this figure the PI capabilities are clearly insufficient as a torque loss of approximately 50% is recorded. In Fig. 13 the same comparison was made at 75% of Ω_l with a low current reference where the same conclusions can be made.

VI. CONCLUSION

An enhanced structure of the hybrid controller was developed. This new structure overcomes drawbacks of the hybrid controller observed with machines with high current dynamics. The proposed controller has been validated by simulation. Theses simulations have proved the effectiveness of the new controller on a wide range of operating speeds. Yet it has been noticed that this controller is sensible to the machine inductance estimation. Further research should be done to treat this problem.

REFERENCES

[1] S. Faid, P. Debal, and S. Bervoets, "Development of a Switched Reluctance Motor for Automotive Traction Applications," in *The 25th World Battery, Hybrid and Fuel Cell Electric Vehicle Symposium & Exhibition*, 2010, pp. 5–9.

[2] H. Hannoun, M. Hilairet, C. Marchand, "Design of an SRM speed control strategy for a wide range of operating speeds," IEEE Transactions on Industrial Electronics, 57 (9), 2911-2921, 2010.

[3] H. Hannoun, M. Hilairet, C. Marchand, "Experimental validation of a switched reluctance machine operating in continuous-conduction mode," IEEE Transactions on Vehicular Technology, 60 (4), 1453-1460, 2011.

[4] X. Ojeda, H. Hannoun, X. Mininger, M. Hilairet, M. Gabsi, C. Marchand, M. Lécrivain, "Switched reluctance machine vibration reduction using a vectorial piezoelectric actuator control," European physical journal. Applied physics, 47 (3), 2009.

[5] H. Hannoun, M. Hilairet, C. Marchand, "Analytical modeling of switched reluctance machines including saturation," IEEE International Electric Machines and Drives Conference (IEMDC), 2007.

[6] H. Hannoun, M. Hilairet, and C. Marchand, "High performance current control of a switched reluctance machine based on a gain-scheduling PI controller," *Control Engineering Practice*, vol. 19, no. 11, pp. 1377–1386, Nov. 2011.

[7] A. V. Rajarathnam, K. M. Rahman, and M. Ehsani, "Improvement of hysteresis control in switched reluctance motor drives," in *IEEE International Electric Machines and Drives Conference. IEMDC'99. Proceedings (Cat. No.99EX272)*, 1999, pp. 537–539.

[8] H. Yang, S. K. Panda, and Y.-C. Liang, "Sliding mode control for switched reluctance motors: an experimental investigation," in *Proceedings of the 1996 IEEE IECON. 22nd International Conference on Industrial Electronics, Control, and Instrumentation*, 1996, vol. 1, pp. 96–101.

[9] G. Espinosa-Perez, P. Maya-Ortiz, M. Velasco-Villa, and H. Sira-Ramirez, "Passivity-Based Control of Switched Reluctance Motors With Nonlinear Magnetic Circuits," *IEEE Transactions on Control Systems Technology*, vol. 12, no. 3, pp. 439–448, May 2004.

[10] M. T. Alrifai, J. H. Chow, and D. A. Torrey, "Practical application of backstepping nonlinear current control to a switched-reluctance motor," in *Proceedings of the 2000 American Control Conference. ACC (IEEE Cat. No.00CH36334)*, 2000, vol. 1, no. 6, pp. 594–599.

[11] J. O. Fiedler, N. H. Fuengwarodsakul, and R. W. De Doncker, "Calculation of switching frequency in current hysteresis controlled switched reluctance drives," in *2004 IEEE 35th Annual Power Electronics Specialists Conference (IEEE Cat. No.04CH37551)*, 2004, vol. 3, pp. 2270–2276.

[12] X. Rain, M. Hilairet, and O. Bethoux, "Comparative study of various current controllers for the switched reluctance machine," in *2010 IEEE Vehicle Power and Propulsion Conference*, 2010, pp. 1–6.

[13] H. J. Brauer, M. D. Hennen, and R. W. De Doncker, "Control for Polyphase Switched Reluctance Machines to Minimize Torque Ripple and Decrease Ohmic Machine Losses," *IEEE Transactions on Power Electronics*, vol. 27, no. 1, pp. 370–378, Jan. 2012.

[14] M. Besbes and B. Multon, "MRVSIM Logiciel de simulation et d'aide à la conception de Machines à réluctance variable à double saillance à alimentation électronique." CNRS, 2004.

.